48th AIAA/ASME/SAE/ASEE Joint Propulsion Conference & Exhibit
30 July - 01 August 2012, Atlanta, Georgia

AIAA 2012-4186

Current Density Measurements of an Annular-Geometry Ion Engine

Rohit Shastry*, Michael J. Patterson†, and Daniel A. Herman‡
NASA Glenn Research Center, Cleveland, OH, 44135

and

John E. Foster§
The University of Michigan, Ann Arbor, MI, 48109

The concept of the annular-geometry ion engine, or AGI-Engine, has been shown to have many potential benefits when scaling electric propulsion technologies to higher power. However, the necessary asymmetric location of the discharge cathode away from thruster centerline could potentially lead to non-uniformities in the discharge not present in conventional geometry ion thrusters. In an effort to characterize the degree of this potential non-uniformity, a number of current density measurements were taken on a breadboard AGI-Engine. Fourteen button probes were used to measure the ion current density of the discharge along a perforated electrode that replaced the ion optics during conditions of simulated beam extraction. Three Faraday probes spaced apart in the vertical direction were also used in a separate test to interrogate the plume of the AGI-Engine during true beam extraction. It was determined that both the discharge and the plume of the AGI-Engine are highly uniform, with variations under most conditions limited to ±10% of the average current density in the discharge and ±5% of the average current density in the plume. Beam flatness parameter measured 30 mm from the ion optics ranged from 0.85 – 0.95, and overall uniformity was shown to generally increase with increasing discharge and beam currents. These measurements indicate that the plasma is highly uniform despite the asymmetric location of the discharge cathode.

Nomenclature

E	=	ion energy
CC	=	cathode centerline
I_b	=	beam current
I_d	=	discharge current
j_b	=	beam current density
N-CC	=	non-cathode centerline
P_d	=	discharge power
r	=	radial distance from thruster centerline
TC	=	thruster centerline
V_b	=	beam power supply voltage
z	=	axial distance downstream of thruster optics
σ_{CEX}	=	charge-exchange collisional cross section between Xe^+ and Xe

* Aerospace Engineer, Propulsion and Propellants Branch, 21000 Brookpark Rd., MS 301-3, AIAA member.
† Senior Technologist, Power and In-Space Propulsion Division, 21000 Brookpark Rd., MS 301-3, AIAA member.
‡‡ Aerospace Engineer, Propulsion and Propellants Branch, 21000 Brookpark Rd., MS 86-8, AIAA senior member.
§ Associate Professor, Department of Nuclear Engineering and Radiological Sciences, 2355 Bonisteel Blvd., AIAA Associate member.

I. Introduction

THE annular-geometry ion engine, or AGI-Engine, is the core technology for a new concept of next-generation electric propulsion thrusters.[1] This technology has been shown to have many potential benefits over conventional ion thrusters when scaling electric propulsion devices to higher power.[1] With the annular geometry, additional anode area is created that allows for operation at much higher discharge currents, translating into higher beam currents. Furthermore, the annular geometry better facilitates the use of pyrolitic graphite for the ion optics. Presently, optics in conventional ion thrusters are domed for thermal expansion stability during operation as well as structural stability during launch. Pyrolitic graphite, which is attractive for its low sputtering yield, can be difficult to properly manufacture in domed configurations. The annular geometry of the AGI-Engine reduces the necessary span-to-gap ratio enough to use flat optics, especially for large beam areas that would otherwise be impractical to implement using conventional geometries. Thus, not only can the annular geometry take advantage of the low wear rate of pyrolitic graphite, but the use of flat optics could also eliminate the divergence of the ion beam that is created by domed ion optics.

While there are many potential benefits to the AGI-Engine, the required location of the discharge cathode away from thruster centerline could create potential non-uniformities in the discharge and plume that would translate into non-uniform or even accelerated wear and possible reduced electron backstreaming margin. In an effort to characterize this potential non-uniformity, a number of current density measurements were taken on a breadboard AGI-Engine. In the first phase of this study, fourteen button probes were placed on a perforated plate which served as the end of the discharge chamber in place of ion optics. Using these probes, the ion current density at various locations in the discharge was measured during conditions of simulated beam extraction.[2] In the second phase of the study, three Faraday probes spaced apart in the vertical direction were swept in the radial direction downstream of the AGI-Engine to characterize the plume at various axial locations during true beam extraction. These measurements were collected over a wide range of discharge powers, beam voltages and beam currents.

The paper is organized as follows: Section II describes the vacuum facility, breadboard AGI-Engine, button probes, and Faraday probes used in this study. Section III first covers the results from the interrogation of the discharge during simulated beam extraction. Profiles of current density are compared across several discharge currents, and the spatial non-uniformity is characterized. The results from the plume interrogation during operation with true beam extraction are then presented and discussed. Representative radial and axial profiles are shown, followed by a discussion of how these profiles changed as a function of beam voltage and current. The radial and azimuthal uniformities of the beam are then characterized. Section IV summarizes the conclusions of the study.

II. Experimental Apparatus

A. Vacuum Facility

This study was conducted within Vacuum Facility 7 (VF-7) at the NASA Glenn Research Center (GRC). Vacuum Facility 7 is a 3-m-diameter by 5.5-m-long cylindrical vacuum chamber equipped with five 0.9-m-diameter oil diffusion pumps. Pressure was monitored using an exposed hot-cathode ionization gauge mounted near the thruster to provide a more accurate measurement of the backpressure that the test article was exposed to during the study. Facility base pressures of 3.3×10^{-6} Pa (2.5×10^{-8} Torr) were routinely achieved. Pressure next to the thruster did not exceed 3.7×10^{-3} Pa (2.8×10^{-5} Torr, corrected for xenon) during testing. While these backpressures are relatively high for ion thruster operation, the calculated neutral ingestion from the facility was limited to 3% of the total discharge mass flow rate. This amount of neutral ingestion is not expected to significantly affect the uniformity or structure of the discharge and plume, and thus was deemed acceptable for preliminary testing of the AGI-Engine.

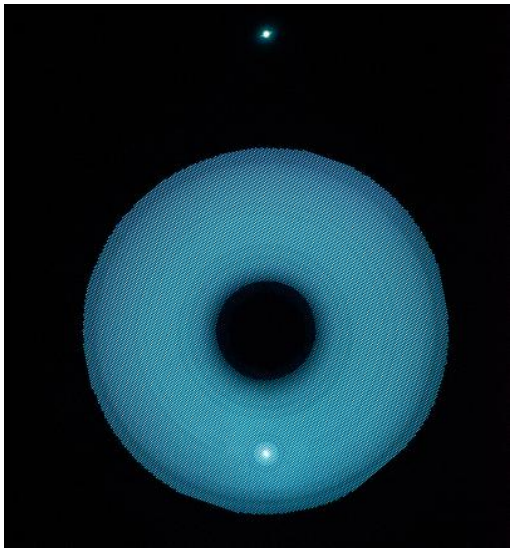

Figure 1. Photograph of the AGI-Engine operating with beam extraction within VF-7.

B. Test Article and Test Support Hardware

The test article for this study is a breadboard model annular-gometry ion thruster that will be referred to as the AGI-Engine (see Fig. 1). Preliminary testing of this thruster under simulated

beam extraction conditions was completed in 2011,[3] while performance measurements with true beam extraction were completed in 2012.[4] The AGI-Engine was designed in collaboration with the University of Michigan, and was fabricated at GRC in 2011 using a combination of components that were originally manufactured for an engineering model (EM) of NASA's Evolutionary Xenon Thruster (NEXT) as well as components specifically built for this test article. The discharge chamber utilized a single hollow cathode located in the radial center of the annulus at the 6 o'clock position. During testing with simulated beam extraction, the discharge chamber was terminated using a perforated plate with an open area fraction equal to the neutral transparency of high-perveance ion optics. This plate was biased at discharge cathode potential for much of the study, and was biased -30 V relative to anode potential to assess ion saturation. During testing with true beam extraction, the thruster was equipped with EM ion optics that were originally manufactured for NEXT. Portions of the ion optics (downstream of the thruster's central anode stalk as well as the outer perimeter of the discharge chamber where plasma density was expected to be low) were masked on the upstream surface of the screen grid using tantalum foil. Additional information on the thruster can be found in Refs. 3-4.

Xenon was supplied using commercially available mass flow controllers with an accuracy of ±1% of the reading. The discharge was sustained using a commercially available power supply capable of supplying 40 V and 60 A. A high-voltage power supply was used to bias the ion optics during testing with true beam extraction. Separate power supplies were used to power the cathode heaters and keepers. Since this study was a preliminary test to compare the performance of the AGI-Engine to state-of-the-art ion thrusters such as NEXT, the thruster was operated using the present NEXT throttling table as a guide throughout the majority of testing. Thus, flow rates and beam voltages were largely dictated by this throttling table in order to make a direct comparison to NEXT performance. Thruster telemetry was monitored throughout testing using calibrated digital multimeters.

C. Discharge Button Probe

In the first phase of this study the AGI-Engine was operated in discharge-only mode under conditions that simulated beam extraction. In order to measure the spatial uniformity of the discharge as well as the ion current density approaching the grid, 14 discharge button probes were mounted at various locations on the perforated grid that enclosed the discharge chamber in place of ion optics. Each planar probe was comprised of a 6.4-mm-diameter disc of molybdenum to minimize secondary electron emission effects.[5] The probes were placed along four radial "lines" to provide data across a wide range of radial and azimuthal positions along the discharge (see Fig. 2). Line "A" was comprised of five probes along the 6 o'clock position, with the middle probe placed downstream of the discharge cathode orifice. Lines "B" and "C" were each comprised of four probes spaced 120° apart from line "A" as well as each other. Line "D" was composed of a single probe spaced 30° from line "A". This configuration allowed for determination of mirror symmetry about the thruster mid-plane passing through the discharge cathode, and of current density sufficiently far away from the discharge cathode to check overall plasma uniformity.

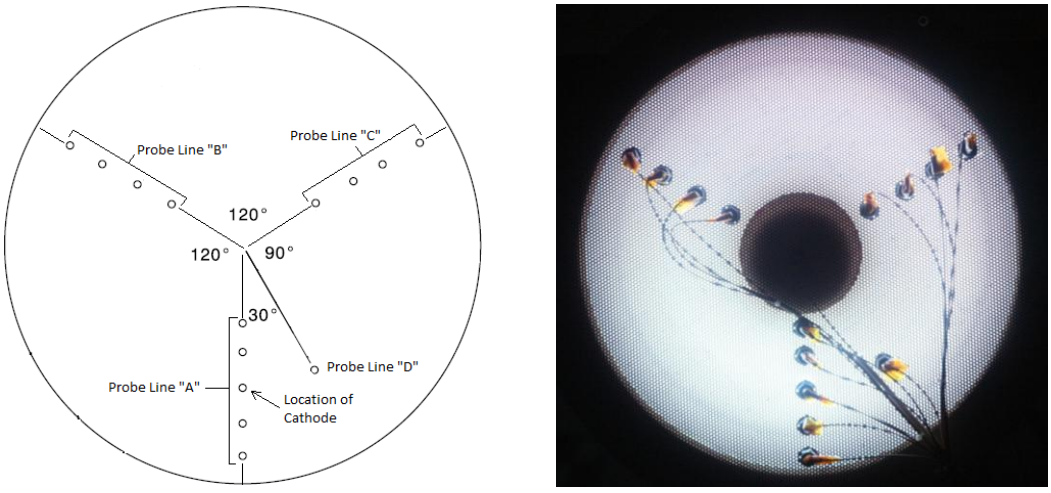

Figure 2. Layout of button probes used to interrogate the discharge of the AGI-Engine during simulated beam extraction. Left: Schematic detailing the orientation and "line" naming convention. Not to scale. Right: Photograph of the AGI-Engine operating with button probes installed on grid.

The current from each probe was measured across a 1000-Ω, 25-W power resistor whose downstream end was connected to a power supply which biased the probes 30 V below anode potential (see Fig. 3). The voltage across each shunt was measured by a 22-channel, 22-bit datalogger connected to a computer. The resistance of each shunt was measured by the datalogger at the beginning of each test day.

Data reduction involved using the measured resistances to calculate the current of each probe from the measured voltages across each shunt using Ohm's law. These currents were then divided by the probe's physical area to determine the ion current density at each location as a function of operating condition. A total of 11 conditions were characterized in this manner. Five of these conditions were taken as representative points from the NEXT throttling table (19 A maximum discharge current). The remaining six conditions were taken between 23 A and 48 A discharge current in order to test the increased current capabilities of the AGI-Engine.

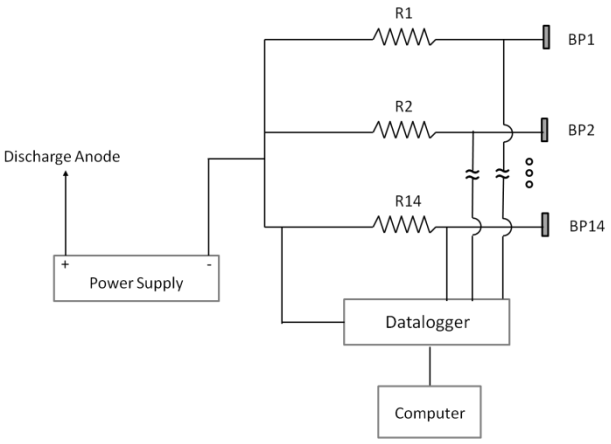

Figure 3. Electrical diagram detailing how currents were measured from the 14 button probes used in this study. "R" corresponds to resistor and "BP" corresponds to button probe.

D. Plume Faraday Probe

In the second phase of this study, the AGI-Engine was run with true beam extraction using a set of EM NEXT ion optics. In order to measure the uniformity and ion beam current density in the plume of the AGI-Engine, an array of three Faraday probes was used. Each Faraday probe was comprised of an 11.1-mm-diameter molybdenum electrode that served as the collector. The collector was surrounded by a stainless-steel shell with an outer diameter of 22.2 mm, which served as a probe guard ring (see Fig. 4). The two electrodes were separated by a insulating collar made of a high-temperature machinable ceramic.

The array of three probes was mounted in the vertical direction such that one probe was in the plane of the thruster centerline, another was in the plane of the discharge cathode centerline, and the last was in the plane of the discharge cathode mirrored about the thruster centerline. Figure 5 shows the Faraday probe array with the AGI-Engine both prior to and during testing with beam extraction. The positions of these probes were selected for two reasons. One was to accommodate traditional interrogation through thruster centerline. The second was to compare the discharge cathode region to its mirror image above the plane of thruster centerline; if azimuthal asymmetries were present, these two regions were expected to contain the largest differences.

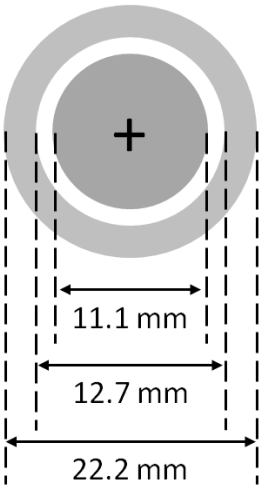

Figure 4. Schematic of the face of the Faraday probe used in this study. Not to scale.

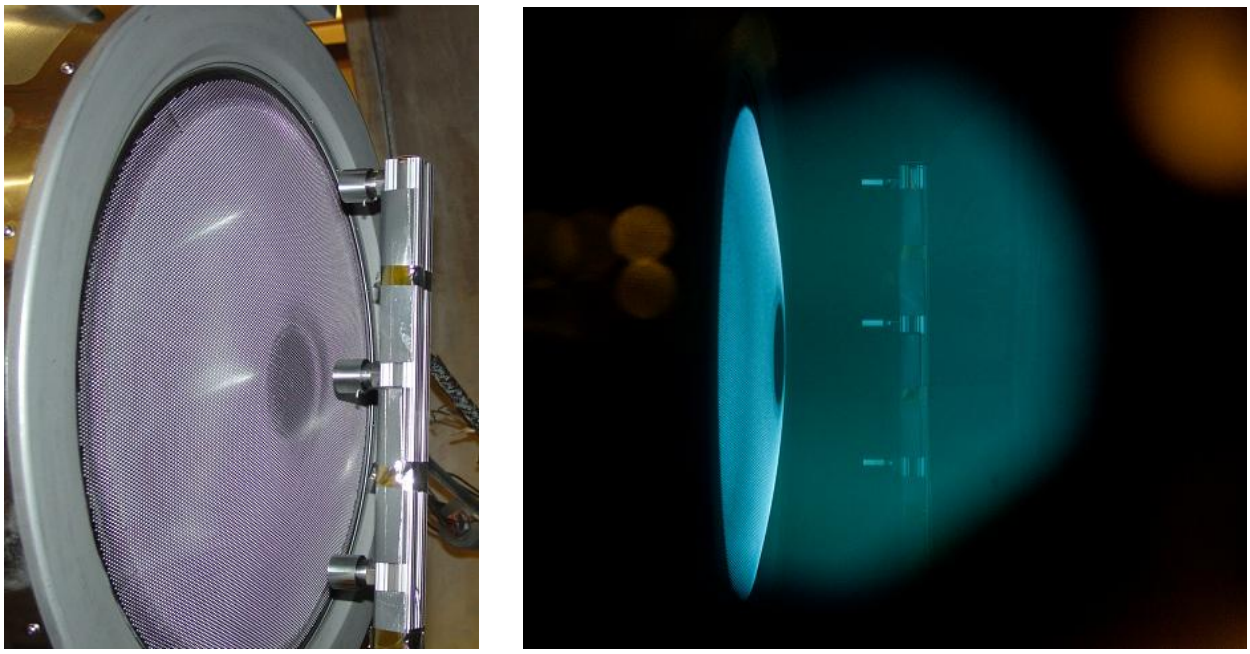

Figure 5. Photographs of the Faraday probe array with the AGI-Engine prior to testing (left) and during testing with beam extraction (right).

The probe array was mounted onto a 2-axis ball-screw driven motion table system that allowed the probes to move approximately ± 600 mm in the radial direction about thruster centerline as well as over 1000 mm downstream of the ion optics in the axial direction. The probe array was swept in the radial direction at approximately 17 mm/s over the full range of motion at four different axial positions: 30 mm, 500 mm, 850 mm, and 1050 mm. These axial positions were measured from the geometric center of the optics to the Faraday probe along thruster centerline, and were chosen to mimic measurement locations from a prior ion current density study performed on NEXT.[6] Scans were also taken in the axial direction in the vertical plane of thruster centerline to characterize how the ion current density decays with downstream distance.

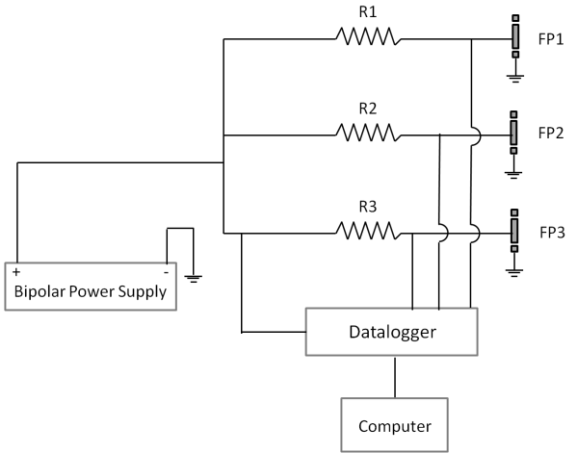

Figure 6. Electrical schematic used to measure currents from the Faraday probes during true beam extraction. "R" corresponds to resistor and "FP" corresponds to Faraday probe.

The current from each Faraday probe was measured across a 1000-Ω, 25-W power resistor whose downstream end was connected to a bipolar power supply which biased each probe to -20 V with respect to facility ground. The voltage across each shunt was monitored using a 22-channel, 22-bit datalogger connected to a computer (see Fig. 6). Data was taken continuously during each radial sweep across the thruster face. Given the finite scan rate of the datalogger, measurements were taken approximately every 3 mm in the radial direction. Due to an uncertainty associated with when the current measurements were taken with respect to position measurements, the average of the positions measured before and after the current measurement was assigned as the position for that measurement. This averaging resulted in a radial position uncertainty of ±1.5 mm.

Each resistor was calibrated by running multiple known currents through it and measuring the voltage drops using the datalogger. These calibration curves, which were found to be linear, were used in post-processing to convert the voltage signals into currents that were then divided by the physical probe areas to obtain ion current densities. As mentioned earlier, operating points for the AGI-Engine were taken from the NEXT throttling table as a guide for establishing a performance map particular to the AGI-Engine . Table 1 gives the NEXT throttle table

and shows the operating conditions where Faraday probe data were successfully obtained. Operating conditions include original throttle levels (TL) as well as extended throttle levels (ETL) beyond the original NEXT throttle table.[4] The extended throttle levels are marked in italics to differentiate them from original throttle levels in Table 1. The number of throttle table operating points actually attainable was limited by the poor original manufacturing quality of the ion optics used (limiting the minimum beam voltage) as well as a high breakdown frequency due to sharp edges on the tantalum foil used to mask off the optics (limiting the maximum beam voltage). Despite these constraints, plume data were obtained at 40 operating conditions across a wide range of beam voltages and currents, which was deemed more than adequate to properly characterize the plume of the AGI-Engine.

Table 1. Operating conditions where plume data during beam extraction were obtained. Conditions that are italicized correspond to extended throttle levels beyond the original NEXT throttle table. Data were successfully collected at a total of 40 operating conditions.

	Beam Power Supply Voltage [V]											
Beam Current [A]	1800	1567	1396	1179	1021	936	850	679	650	400	300	275
3.52	TL40	TL39	TL38	TL37	*ETL3.52A*	*ETL3.52B*	*ETL3.52C*					
3.10	TL36	TL35	TL34	TL33	*ETL3.1A*	*ETL3.1B*	*ETL3.1C*	*ETL3.1E*				
2.70	TL32	TL31	TL30	TL29	TL28	*ETL2.7A*	*ETL2.7B*	*ETL2.7D*	*ETL2.7E*			
2.35	TL27	TL26	TL25	TL24	TL23	*ETL2.35A*	*ETL2.35B*	*ETL2.35D*	*ETL2.35E*			
2.00	TL22	TL21	TL20	TL19	TL18	*ETL2.0A*	*ETL2.0B*	*ETL2.0D*	*ETL2.0E*			
1.60	TL17	TL16	TL15	TL14	TL13	*ETL1.6A*	*ETL1.6B*	*ETL1.6D*	*ETL1.6E*	*ETL1.6F*		
1.20	TL12	TL11	TL10	TL09	TL08	TL07	TL06	TL05	TL04	TL03	TL02	
1.00												TL01

Data Collected | Not Part of Throttling Table

III. Results and Discussion

Ion current density measurements were taken on the breadboard AGI-Engine in an effort to determine the spatial uniformity of the discharge as well as the plume. In the first phase of the study, 14 button probes were used to measure ion current density at the perforated grid at conditions that simulated beam extraction. In the second phase, three Faraday probes were used to interrogate the plume at four downstream distances from the thruster during true beam extraction. The results of these measurements are presented in this section. Uniformity of the both the discharge and the plume as a function of operating condition is also discussed.

A. Discharge Measurements

Fourteen button probes placed at various radial and azimuthal locations were used to measure the ion current density of the discharge at the 11 different operating points shown in Table 2. The first five operating conditions represent various throttle levels taken from the NEXT throttle table (see Table 1). The remaining six conditions continue to push the discharge current beyond NEXT throttle levels, as high as 48 A.

Figure 7 shows representative profiles from four of the 11 operating conditions tested during simulated beam extraction. The distance bounds in each plot correspond to the anode surfaces within the discharge chamber. These profiles show that, under most conditions, the discharge is highly uniform within the "bulk" plasma (away from the anode walls). Signficant overlap in measured current between probe lines "B" and "C" also suggest a high degree of azimuthal symmetry. Measured current densities in this region varied from 1.1 – 8.2 mA/cm^2, depending on operating condition. At certain operating points, the current density measured downstream of the discharge cathode (r = 12.5 cm along probe line "A") was significantly higher than surrounding locations. This feature appeared primarily when operating at higher discharge currents (≥ 38 A). This increased peakedness is believed to be caused by the cathode plume at higher discharge currents creating more localized plasma, which can diffuse more easily downstream towards the perforated plate. Also seen in Fig. 7, the current density appears to fall rather rapidly within 2 cm of the anode surface. There are two possible reasons for this drop in measured current density. One is that these regions are downstream of the portion of the discharge containing strong magnetic fields, naturally resulting in a much lower plasma density. The second reason is that the probe itself was positioned rather close to the edge of the discharge. Given the size of the probe (6.4 mm diameter), portions of it may have been shadowed by

various supporting structures in the vicinity of the anode wall, effectively reducing its collection area. Regardless, the ion optics used during beam extraction were masked off at these radial locations due to the low expected current density, and thus these regions should not affect the uniformity of the plume. For these reasons, the measured current densities near the anode walls are not included when calculating properties of the overall discharge.

Table 2. List of operating conditions tested during simulated beam extraction, as well as the corresponding discharge powers. The representative throttle level refers to the NEXT throttle table, which is shown in Table 1.

Representative Throttle Level	Discharge Current [A]	Discharge Power [W]
ETL1.6F – TL17 (I_b = 1.60 A)	12.4	239
ETL2.0E – TL22 (I_b = 2.00 A)	13.9	263
ETL2.7E – TL32 (I_b = 2.70 A)	15.3	330
ETL3.1E – TL36 (I_b = 3.1 A)	17.1	367
ETL3.52C – TL40 (I_b = 3.52 A)	18.9	399
--	23.9	584
--	28.0	686
--	33.0	796
--	38.0	874
--	43.0	902
--	48.0	918

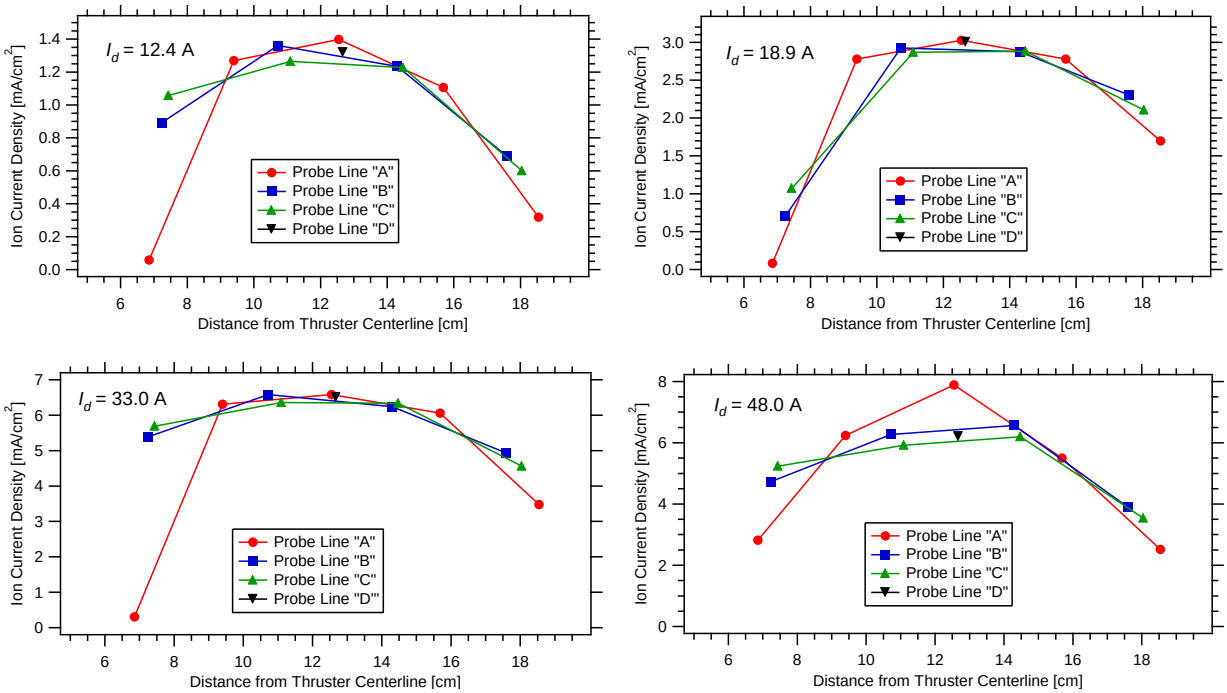

Figure 7. Representative current density profiles along the perforated plate while operating the AGI-Engine under simulated beam extraction. Under most operating conditions, the discharge appears to be highly uniform in the central area of the annulus. Distance bounds correspond to the anode walls.

In order to quantify the degree of non-uniformity within the bulk plasma of the discharge, the variation in measured ion current densities is defined as

$$\% \text{ Non-Uniformity} = \frac{(j_{b,max} - j_{b,min})/2}{(j_{b,max} + j_{b,min})/2} \times 100, \quad (1)$$

where j_b is the measured ion current density. When calculating non-uniformity of the discharge, the outer probes (near the anode walls) of each probe line were omitted as previously discussed. Figure 8 shows the calculated discharge non-uniformities for the 11 operating conditions tested under simulated beam extraction. All non-uniformities were within ±20%, with many less than ±7%. The cause of the spike in non-uniformity at a discharge current of 15.3 A (discharge power of 330 W) is presently unknown. The discharge appeared most unifom at moderate discharge currents and powers. This was confirmed with plume measurements presented in Section III-B. The rise in non-uniformity at higher discharge powers is primarily due to the increased peakedness in current density by the discharge cathode. However, this rise in non-uniformity remains even if the measured current density downstream of the discharge cathode is not included in the calculation, indicating another cause that is presently unknown.

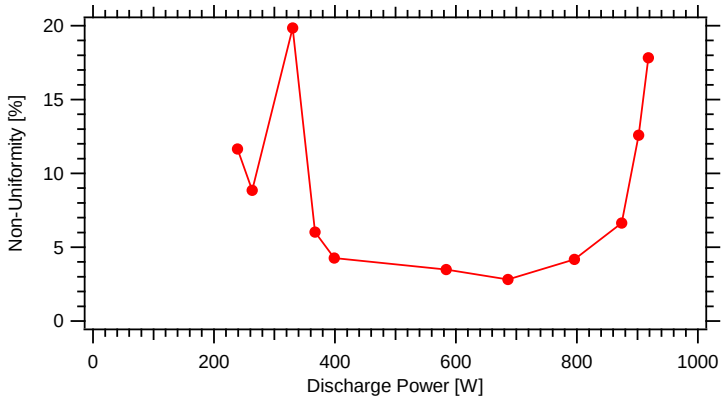

Figure 8. Non-uniformity of the bulk discharge plasma as a function of discharge power. All conditions tested exhibited non-uniformities ≤ ±20%, with most conditions exhibiting excellent uniformity (non-uniformity ≤ ±7%).

Using the same restrictions on data points as the non-uniformity calculation, the average measured current density in the bulk plasma was calculated as a function of discharge power (see Fig. 9). As seen in the figure, current densities as high as 7.1 mA/cm^2 were measured in the bulk plasma. The reason for the dropoff at I_d = 48 A (P_d = 918 W) is presently unknown. While the average current density appears to be fairly linear with discharge power, the discharge losses were found to be much lower at higher powers during simulated and true beam extraction.[3,4] This is consistent with findings here that show equivalent losses as high as 190 W/mA-cm^{-2} at lower discharge powers and as low as 125 W/mA-cm^{-2} at the higher discharge powers.

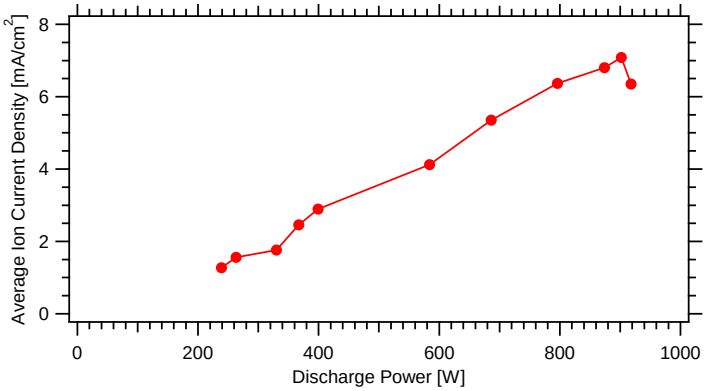

Figure 9. Average ion current density along the perforated grid during conditions of simulated beam extraction. Average current densities as high as 7.1 mA/cm^2 were calculated in the bulk plasma of the discharge.

One interesting feature of note is that the uniformity of the discharge plasma appeared to be a strong function of the anode mass flow rate. As part of the procedure for simulating beam extraction, the mass flow rate was initially set at the nominal value used during true beam extraction, then reduced until the measured ion current to the

perforated grid maximized. Figure 10 compares the ion density profiles along the perforated grid between the "flooded" case (nominal anode mass flow rate) and "leaned" case (reduced mass flow rate to simulate beam extraction) at a discharge current of 38 A. The figure shows that not only does leaning out the mass flow increase the ion current density to the grid, but it also significantly improves spatial uniformity of the discharge plasma. The theorized mechanism for plasma uniformity in the AGI-Engine is an electron drift motion in the azimuthal direction due to radial gradients in the magnetic field. If this is the case, then a significantly higher collision frequency within the discharge chamber (due to excessive mass flow) could result in enhanced diffusion of electrons, increasing the likelihood they are lost to the anode before they have the opportunity to drift azimuthally around the chamber. This excessive collisionality would reduce the effectiveness of the electron drift motion and cause an increase in spatial non-uniformity. However, for neutral pressures within the discharge that are representative of true beam extraction, the plasma appears to be highly uniform in the breadboard AGI-Engine.

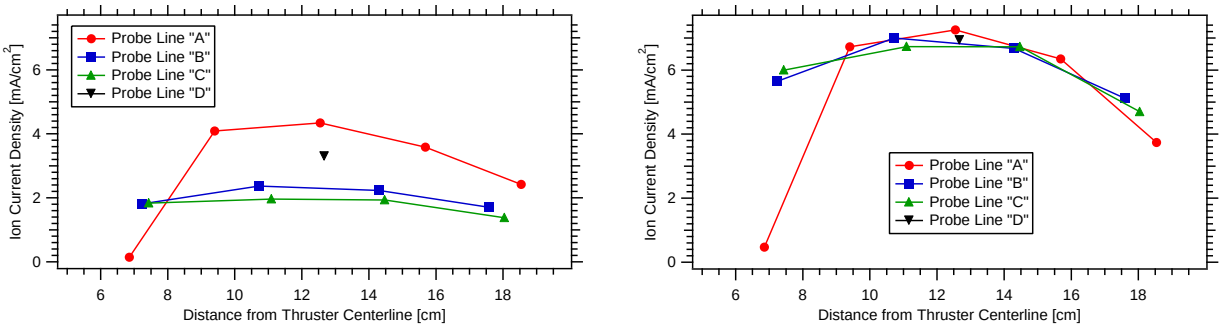

Figure 10. Comparison of measured ion curret densities along the perforated grid between "flooded" (left) and "leaned" (right) mass flow rate conditions at I_d = 38 A. Not only does the reduction in flow rate increase the current density to the grid, but also significantly increases spatial uniformity of the discharge.

B. Plume Measurements

Three Faraday probes spaced apart in the vertical direction were used to interrogate the plume of the breadboard AGI-Engine. Scans were taken in the radial direction ±600 mm from thruster centerline at four axial locations: 30 mm, 500 mm, 850 mm, and 1050 mm from the ion optics. Scans were also taken in the axial direction within the vertical plane of thruster centerline in order to characterize how the ion current density evolved with downstream distance from the thruster. Ion current density profiles in the radial direction will have the following nomenclature: data taken in the plane of the thruster centerline will be labeled "thruster centerline" or "TC"; data taken in the plane of the discharge cathode will be labeled "cathode centerline" or "CC"; and data taken in the cathode plane mirrored about thruster centerline will be labeled "non-cathode centerline" or N-CC."

Representative current density profiles will be presented first to illustrate the general shape and evolution of the plasma plume of the AGI-Engine. Comparisons will then be made between the radial profiles in the plane of thruster centerline at z = 30 mm for various operating conditions. Spatial uniformity across operating conditions will then be presented and discussed.

1. Representative Ion Current Density Profiles

Figure 11 shows radial profiles of ion current density at V_b = 1179 V, I_b = 3.52 A for the four different axial locations. Values are plotted on a log scale to better illustrate the profile shape evolution with downstream distance. Profiles taken within the plane of thruster centerline exhibit a double-hump structure due to the annular geometry of the discharge chamber. This structure is very distinct at z = 30 mm from the ion optics, but flattens with downstream distance as the plume expands into a more uniform beam. Since the profile within the plane of the discharge cathode does not include the central area of inactive optics, a much flatter, single hump structure is seen at z = 30 mm from the ion optics. It is interesting to note that despite passing downstream of the discharge cathode, no corresponding pronounced peak in the current density is seen at this location. The profiles in this plane begin to resemble the profiles at thruster centerline as downstream distance increases. This occurs because each probe can collect current from more grid apertures as downstream distance increases, due to the limited maximum angle at which ions exit the thruster apertures. Thus, at large axial distances all three probes are able to "see" current from the entire thruster and thus measure similar current densities.

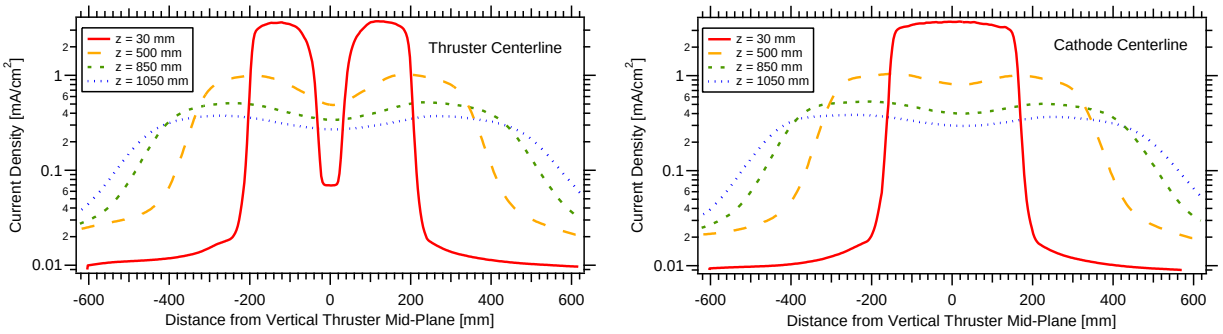

Figure 11. Radial profiles of ion current density as a function of distance from the ion optics within planes of thruster centerline (left) and cathode centerline (right). While the profiles have distinct shapes between the two planes at *z* = 30 mm from the optics, they begin to show similarity as downstream distance increases.

Figure 12 compares radial profiles at V_b = 1179 V, I_b = 3.52 A within the three interrogated planes at z = 30 mm from the ion optics. Current densities are plotted on a log scale to illustrate rapid falloffs, which were found to align closely with the edges of the active ion optics. As seen before in Fig. 11, the profile within the thruster centerline plane exhibits a double-hump structure while the other two do not. It should be stressed that the two profiles within the planes of cathode and non-cathode centerline exhibit a high degree of similarity, despite the fact that one is downstream of the discharge cathode and the other is on the opposite side of the thruster. This comparison is better illustrated in Fig. 13, which plots the current densities on a linear scale and focuses on the region directly downstream of the ion optics. The figure clearly shows that the radial profiles through cathode centerline and non-cathode centerline are not only similar to each other but also exhibit a high degree of beam flatness. Peak current densities for all three profiles were also found to be very close to each other, indicating a high-degree of azimuthal uniformity. These characteristics will be better quantified and characterized across operating conditions in Section III-B-3.

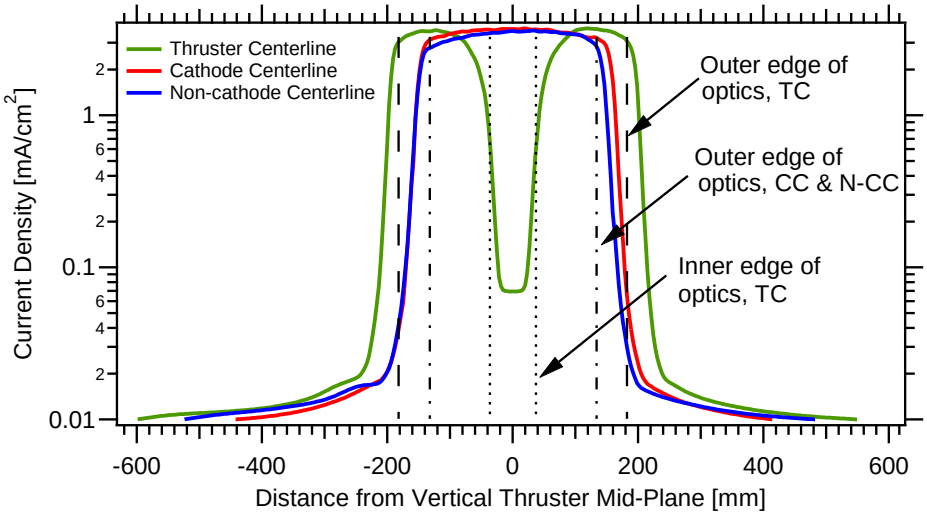

Figure 12. Comparison of radial profiles within the three interrogated planes at *z* = 30 mm from the ion optics. Ion current densities are plotted on a log scale in order to illustrate the sharp decreases associated with the edges of the optics extraction area. Measured profiles within the plane of the discharge cathode and non-discharge cathode were found to be highly similar.

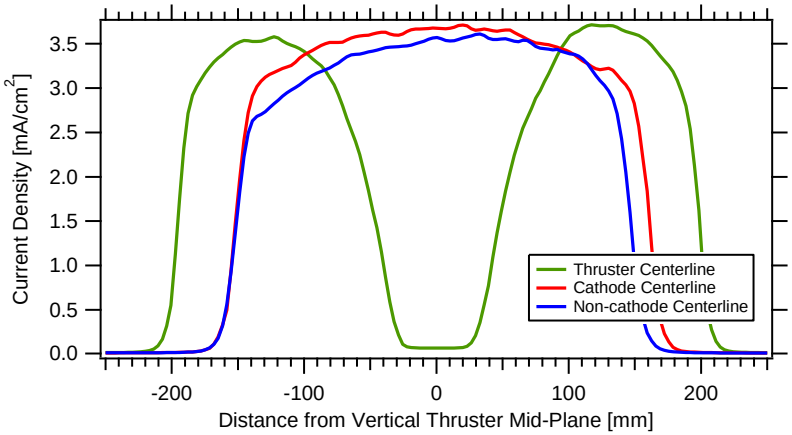

Figure 13. Comparison of radial profiles within the three interrogated planes at z = 30 mm from the ion optics. Current densities are plotted on a linear scale and distances are limited to the vicinity of thruster centerline in order to more accurately illustrate the structure of the plume in this region. Across the three profiles, a high degree of beam flatness and uniformity is seen.

Figure 14 shows the axial profiles of ion current density along thruster, cathode and non-cathode centerlines at V_b = 1179 V and I_b = 3.52 A. As seen before, the profiles along cathode centerline and non-cathode centerline exhibit a high degree of similarity. Both of these profiles were found to decay exponentially with downstream distance. The profile along thruster centerline, however, shows much more structure due to the central area of inactive optics. The initial rise in current density is believed to be the result of the two sides of the beam merging together along thruster centerline. The subsequent falloff in current density with distance is likely due to geometric expansion effects beginning to dominate once the beam has merged. This simple picture is complicated with the effects of charge-exchange (CEX) collisions in the plume. Since the region near the inactive optics has a relatively low plasma density, it is also expected to have a low plasma potential. Thus, CEX ions in the plume will be drawn radially in towards thruster centerline (see Fig. 15). While some of these ions are expected to move upstream towards the negatively-biased accelerator grid, many are expected to move downstream. The exact nature of CEX ion movement in this region is unknown. Thus, while beam merging (and beam divergence) is expected to be the primary factor in shaping the axial profile along thruster centerline, CEX ions are also expected to contribute to its structure. Measurements of the plasma potential and/or use of a gridded Faraday probe in this region, which would help further illuminate how the CEX population affects the ion current density close to thruster centerline, is left for future work.

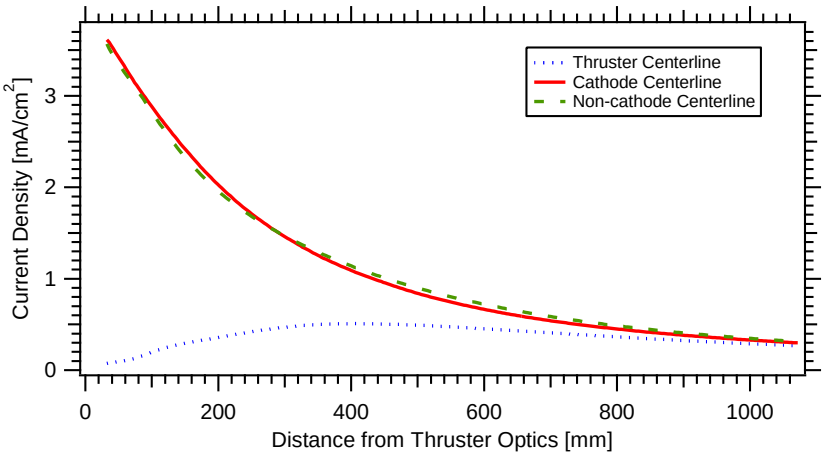

Figure 14. Axial profiles of ion current density along thruster, cathode, and non-cathode centerlines. Cathode centerline and non-cathode centerline profiles were found to be highly similar and decay exponentially with distance. The profile along thruster centerline shows an increase in current density before decay, indicating the beams from either sides of the thruster merge in the center before geometric expansion effects begin to dominate.

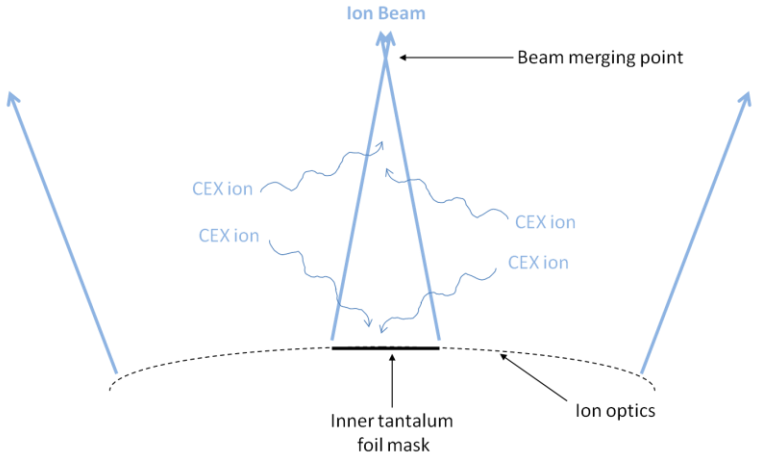

Figure 15. Illustration of various phenomena that affect the axial current density profile along thruster centerline. While the primary effect is expected to come from the two sides of the beam merging in the center, CEX ions from the plume are also expected to populate this region that is characterized by a low plasma potential.

2. Comparisons at Constant Beam Voltage and Current

In order to illustrate how the plume structure varies with operating condition, comparisons will now be made between radial profiles taken within the plane containing the thruster centerline at constant beam power supply voltage as well as constant beam current. Figure 16 shows the radial profiles at a constant beam current of 1.20 A. Values have been plotted on a log scale to better illustrate behavior away from the location of peak current density. On the inner side of this peak, the current density decreases more gradually and has a higher value at thruster centerline at lower voltages. On the outer side of the peak, however, the current density drops off most rapidly at moderate beam voltages around 679 V. The reason for this is due to a combination of beam divergence and CEX population effects. Previous measurements on NEXT using a similar set of ion optics have shown that at a beam current of 1.20 A, the beam divergence was minimized at a beam voltage of 679 V.[6] This is consistent with the data on the outer side of the peak current density, which shows the most rapid falloff occurring around 679 V – a more rapid falloff is indicative of a more collimated beam. Thus, the trend on the outer side of the profile is attributed to beam divergence effects. As mentioned in the previous section, however, the evolution of current density along thruster centerline is affected by how quickly the two sides of the ion beam merge in the center (i.e. how divergent they are) and how CEX ions populate the central area characterized by low density and plasma potential. Since the trends on the inner and outer sides of the profile do not match, the inner side is likely more affected by CEX effects. While the neutral density in the plume is not expected to change significantly since the mass flow rates remain unchanged, the CEX collisional cross section is a function of the ion energy[7] (and thus also beam voltage):

$$\sigma_{CEX} = 87.3 - 13.6log(E), \tag{2}$$

where σ_{CEX} is the collisional cross section for charge-exchange collisions between singly-ionized xenon and neutrals (in units of 10^{-20} m^2), and E is the ion energy in eV. While there is not a significant change in cross section with ion energy, increased CEX collisions are expected to occur at lower ion energies and beam voltages. This dependence on voltage would explain the trend seen on the inner side of the profiles in Fig. 16. It should be noted that since these values are plotted on a log scale, the actual variation (outside of 300 and 400 V) is rather small. However, the trend with beam voltage does indicate that CEX effects may have a significant impact on the structure of the ion current density in the vicinity of thruster centerline.

Figure 17 shows the radial profiles of ion current density in the plane of thruster centerline at a constant beam power supply voltage of 1179 V. Values at each condition have been normalized by the average beam current density for a more direct comparions between profiles. While not easily seen in the figure, the peak (normalized) current density was found to decrease with increasing beam current. However, the current density dropoff on the outer side of the profile occurs more rapidly at higher beam currents. This is consistent with previous measurements on NEXT using a similar set of ion optics, which showed that beam divergence decreased with increasing beam

current at 1179 V.[6] Figure 17 shows that the dropoff also occurs further from thruster centerline at higher beam currents, an indication that the beam itself is flatter at these conditions.

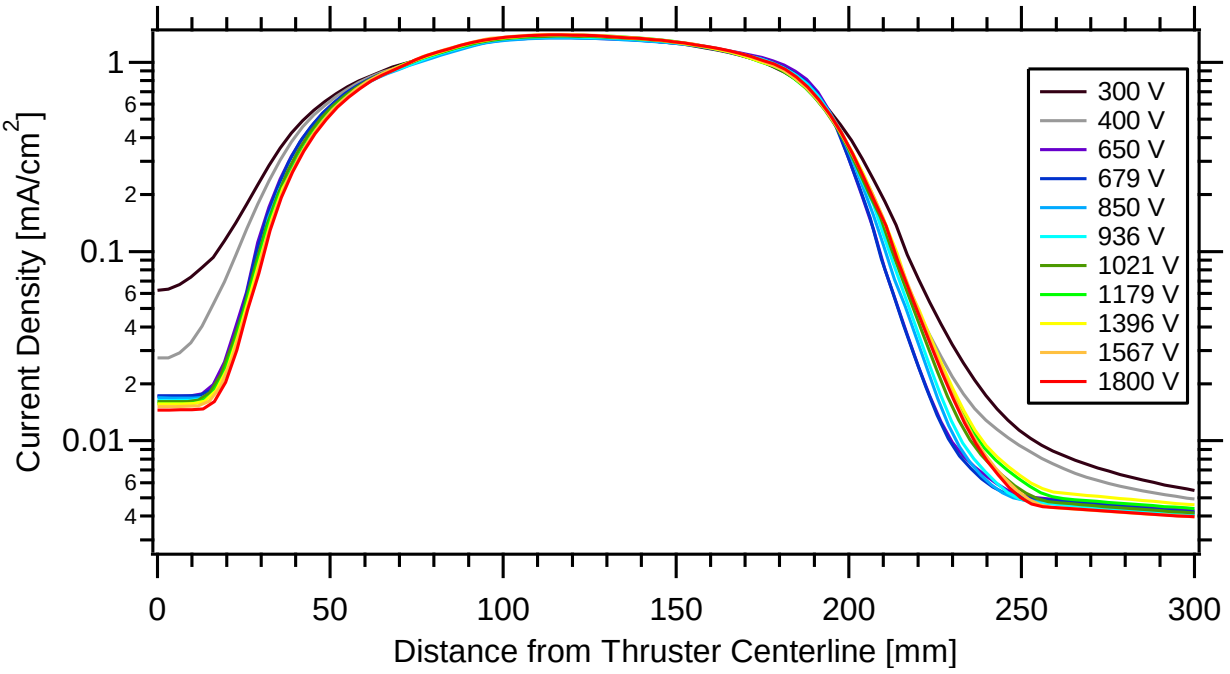

Figure 16. Radial profiles of ion current density within the plane containing the thruster centerline at *z* = 30 mm and a constant beam current of 1.20 A. The current density at thruster centerline is strongly affected by charge-exchange ions, while the dropoff on the outer edge of the beam is dictated by beam divergence.

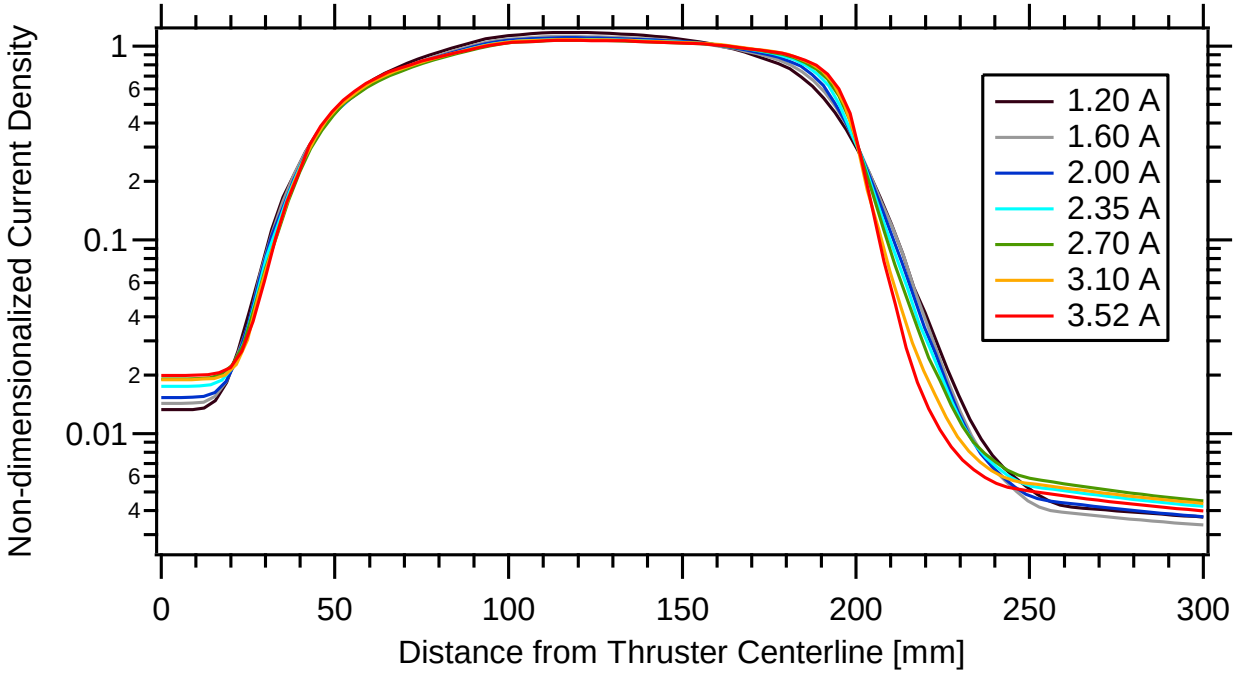

Figure 17. Radial profiles of ion current density in the plane containing the thruster centerline at *z* = 30 mm and a constant beam power supply voltage of 1179 V. Profiles have been non-dimensionalized by average beam current density to allow for a more direct comparison. The current density at thruster centerline is influenced by charge-exchange ions, while the dropoff on the outer side of the beam is affected by beam divergence and flatness.

The normalized value of current density at thruster centerline monatonically increases with increasing beam current. CEX collisions in the plume were previously shown to have a significant effect on the plasma close to thruster centerline. This increase in measured current density in the central region is attributed to increased CEX collisions from a higher neutral density in the plume, which naturally occurs due to the increased mass flow rates associated with higher beam currents. The structure of the ion current density profiles have been shown once again to be affected by CEX collisions as well as the beam divergence.

3. Beam Flatness and Uniformity

In order to quantify the degree of radial and azimuthal uniformity within the plume of the AGI-Engine, the beam flatness parameter was calculated along with an azimuthal non-uniformity percentage based on Eq. (1). All values used correspond to an axial location of 30 mm from the thruster optics. For azimuthal non-uniformity, four locations were compared to characterize the degree of variation: at r = 12.5 cm (radial location of discharge cathode) at 3, 6, 9, and 12 o'clock positions. Figure 18 shows the calculated azimuthal non-uniformity as a function of current for selected beam power supply voltages. All calculated values were found to be $\leq \pm 5\%$, indicating a high-degree of uniformity. Azimuthal uniformity appears to increase with increasing beam current – values as low as 1-2% non-uniformity were calculated at these conditions. The uniformity of the AGI-Engine was of critical importance to verify given the asymmetric location of the discharge cathode. Results shown in Fig. 18 show that despite the asymmetric geometry, azimuthal uniformity is not compromised for the conditions tested. Calculated azimuthal uniformities for all tested operating conditions can be found in the appendix.

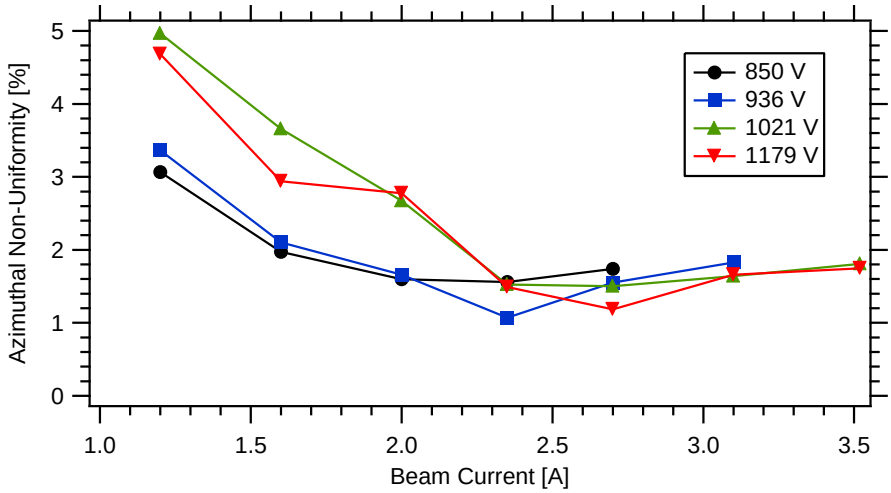

Figure 18. Calculated azimuthal non-uniformity as a function of beam current. Uniformity appears to improve with increasing beam current. Measured non-uniformities did not exceed ±5% for all operating conditions tested.

Radial uniformity is characterized using the beam flatness parameter, defined as the average beam current density divided by the maximum measured ion current density. The average current density is calculated by dividing the beam current by the beam extraction area. The curvature of the optics was accounted for when determining this area. The maximum measured current density was determined from the average of the maximum measured in the plane of cathode centerline, in the plane of non-cathode centerline, and at the 3 o'clock and 9 o'clock positions in the plane of thruster centerline, all at a distance of z = 30 mm from the ion optics. Figure 19 shows the calculated beam flatness parameter as a function of beam current for selected beam power supply voltages. Flatness generally increases with increasing beam current, like the calculated azimuthal uniformity. Values between 0.85 and 0.95 were found across all 40 operating conditions tested (see appendix), indicating a high-degree of radial uniformity. Overall, the plume was found to be highly uniform and symmetric across a wide range of beam voltages and currents.

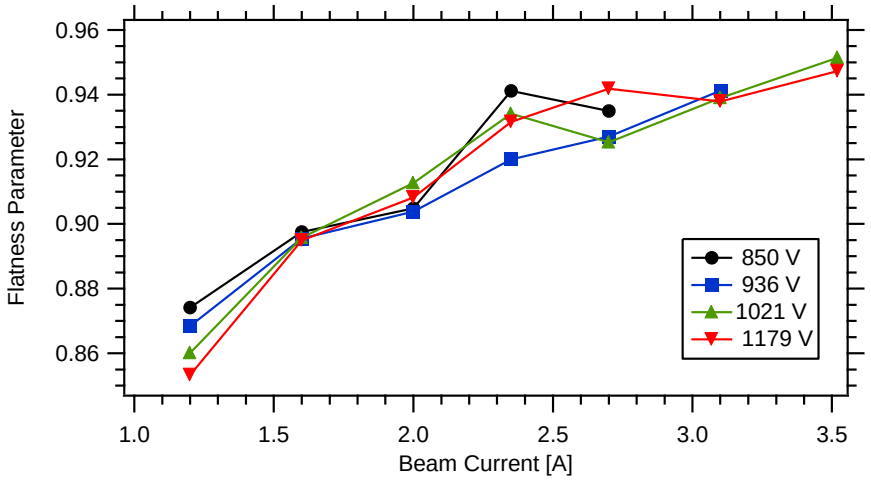

Figure 19. Calculated beam flatness parameter as a function of beam current. Flatness (and thus uniformity) was found to increase with beam current.

IV. Conclusions

In an effort to characterize the degree of non-uniformity in the discharge and plume of the breadboard AGI-Engine, 14 button probes were used to measure the ion current density of the discharge along a perforated plate that took the place of ion optics during conditions of simulated beam extraction. Three Faraday probes spaced apart in the vertical direction were also used in a separate test to interrogate the plume at four axial locations downstream of the ion optics during true beam extraction. These measurements have shown that over a wide range of discharge powers, beam voltages and beam currents, the discharge and plume of the AGI-Engine is highly uniform. For most operating conditions, non-uniformities in the discharge did not exceed ±10%, while non-uniformities in the plume did not exceed ±5%. Beam flatness parameter calculated at 30 mm from the ion optics was found to vary between 0.85 and 0.95, with uniformity generally increasing with increasing discharge and beam currents. The uniformity of the discharge appeared to be a strong function of mass flow rate, with excessive neutral pressures within the discharge chamber disrupting the effectiveness of the azimuthal electron drift that is theorized to be the source of plasma uniformity in the AGI-Engine. The shape of radial profiles of ion current density near the ion optics was found to be primarily affected by the beam divergence as well as CEX populations within the plume. Overall this study has found that despite the asymmetric location of the discharge cathode, both the discharge and plume of the AGI-Engine are highly uniform.

Appendix

Table A1. Calculated azimuthal non-uniformities and flatness parameters for all 40 operating conditions tested with true beam extraction. Throttle level refers to the NEXT throttle table found in Table 1.

Throttle Level	V_b [V]	I_b [A]	Azimuthal Non-Uniformity [%]	Flatness Parameter
TL01	275	1.00	2.3	0.87
TL02	300	1.20	3.6	0.87
TL03	400	1.20	3.5	0.88
TL04	650	1.20	3.1	0.88
TL05	679	1.20	5.1	0.87
TL06	850	1.20	3.1	0.87
TL07	936	1.20	3.4	0.87
TL08	1021	1.20	5.0	0.86
TL09	1179	1.20	4.7	0.85
TL10	1396	1.20	3.3	0.86
TL11	1567	1.20	3.6	0.86
TL12	1800	1.20	3.9	0.86
ETL1.6D	679	1.60	3.6	0.91
ETL1.6B	850	1.60	2.0	0.90
ETL1.6A	936	1.60	2.1	0.90
TL13	1021	1.60	3.7	0.90
TL14	1179	1.60	2.9	0.90
TL15	1396	1.60	2.2	0.89
TL16	1567	1.60	2.5	0.89
ETL2.0D	679	2.00	2.5	0.92
ETL2.0B	850	2.00	1.6	0.91
ETL2.0A	936	2.00	1.7	0.90
TL18	1021	2.00	2.7	0.91
TL19	1179	2.00	2.8	0.91
TL20	1396	2.00	1.7	0.92
TL21	1567	2.00	1.8	0.91
ETL2.35B	850	2.35	1.6	0.94
ETL2.35A	936	2.35	1.1	0.92
TL23	1021	2.35	1.5	0.93
TL24	1179	2.35	1.5	0.93
TL25	1396	2.35	1.3	0.93
ETL2.7B	850	2.70	1.7	0.94
ETL2.7A	936	2.70	1.6	0.93
TL28	1021	2.70	1.5	0.93
TL29	1179	2.70	1.2	0.94
ETL3.1B	936	3.10	1.8	0.94
ETL3.1A	1021	3.10	1.6	0.94
TL33	1179	3.10	1.7	0.94
ETL3.52A	1021	3.52	1.8	0.95
TL37	1179	3.52	1.7	0.95

Acknowledgments

The authors would like to acknowledge and thank George Soulas for fruitful discussion and Kevin McCormick for aiding in the experimental setup. The authors would also like to thank Donna Rizer, Rich Polak, and Jim Schneider for operating and maintaining the facility used in this study. The research presented in this paper was supported under a Center Innovation Fund (CIF) at the National Aeronautics and Space Administration Glenn Research Center at Lewis Field.

References

[1]Patterson, M. J., "Next-Generation Electric Propulsion Thrusters," Presented at the 47th AIAA/ASME/SAE/ASEE Joint Propulsion Conference & Exhibit, AIAA-2011-5812, San Diego, CA, July 31 - August 3, 2011.

[2]Brophy, J. R., "Simulated Ion Thruster Operation Without Beam Extraction," Presented at the 21st International Electric Propulsion Conference, AIAA-1990-2655, Orlando, FL, July 18-20, 1990.

[3]Patterson, M. J., Herman, D. A., Shastry, R., Vannoord, J. L., and Foster, J. E., "Development of an Annular-Geometry Ion Engine," Presented at the Space Propulsion 2012, Conference Paper 2356236, Bordeaux, France, May 7 - 10, 2012.

[4]Patterson, M. J., Herman, D. A., Shastry, R., Vannoord, J. L., and Foster, J. E., "Annular-Geometry Ion Engine: Concept, Development Status, and Preliminary Performance," Presented at the 48th AIAA/ASME/SAE/ASEE Joint Propulsion Conference and Exhibit, Atlanta, GA, July 29 - August 1, 2012.

[5]Hagstrum, H. D., "Auger Ejection of Electrons from Molybdenum by Noble Gas Ions," *Physical Review* 104, 3, 672 - 683 (1956).

[6]Pollard, J. E., Diamant, K. D., Crofton, M. W., Patterson, M. J., and Soulas, G. C., "Spatially-Resolved Beam Current and Charge-State Distributions for the NEXT Ion Engine," Presented at the 46th AIAA/ASME/SAE/ASEE Joint Propulsion Conference and Exhibit, AIAA-2010-6779, Nashville, TN, July 25-28, 2010.

[7]Shastry, R., Hofer, R. R., Reid, B. M., and Gallimore, A. D., "Method for Analyzing ExB Probe Spectra from Hall Thruster Plumes," *Review of Scientific Instruments* 80, 6, 063501-1 - 063502-11 (2009).